Article

New Studies of the Physical Properties of Metallic Amorphous Membranes for Hydrogen Purification

Oriele Palumbo [1], Francesco Trequattrini [1,2], Suchismita Sarker [3], Madhura Hulyakar [3], Narendra Pal [3], Dhanesh Chandra [3], Michael Dolan [4] and Annalisa Paolone [1,*]

[1] Consiglio Nazionale delle Ricerche, Istituto dei Sistemi Complessi, U.O.S. La Sapienza, Piazzale A. Moro 5, 00185 Roma, Italy; oriele.palumbo@roma1.infn.it (O.P.); francesco.trequattrini@roma1.infn.it (F.T.)
[2] Department of Physics, Sapienza University of Rome, Piazzale A. Moro 5, 00185 Roma, Italy
[3] Department of Chemical and Materials Engineering, University of Nevada, Reno, NV 89557, USA; suchismita13994@gmail.com (S.S.); hulyalkar.madhura@gmail.com (M.H.); narendrakpal@gmail.com (N.P.); dchandra@unr.edu (D.C.)
[4] Commonwealth Scientific and Industrial Research Organisation, Queensland Centre for Advanced Technologies, Energy, 1 Technology Court, Pullenvale, QLD 4069, Australia; Michael.Dolan@csiro.au
* Correspondence: annalisa.paolone@roma1.infn.it; Tel.: +39-06-4991-4400

Abstract: Amorphous metallic membranes display promising properties for hydrogen purification up to an ultrapure grade (purity > 99.999%). The hydrogen permeability through amorphous membranes has been widely studied in the literature. In this work we focus on two additional properties, which should be considered before possible application of such materials: the propensity to crystallize at high temperatures should be avoided, as the crystallized membranes can become brittle; the hydrogen solubility should be high, as solubility and permeability are proportional. We investigate the crystallization process and the hydrogen solubility of some membranes based on Ni, Nb, and Zr metals, as a function of Zr content, and with the addition of Ta or B. The boron doping does not significantly affect the crystallization temperature and the thermal stability of the membrane. However, the hydrogen solubility for p ~7 bar is as high as H/M ~0.31 at T = 440 °C and H/M ~0.27 at T = 485 °C. Moreover, the membrane does not pulverize even after repeated thermal cycles and hydrogenation processes up to 485 °C and 7 bar, and it retains its initial shape.

Keywords: amorphous membranes; hydrogen purification; hydrogen solubility; crystallization

1. Introduction

Hydrogen purification by using membranes is needed in many industrial applications [1]. In some fields, such as the electronic industry or for feeding fuel cells, a hydrogen gas of an ultrapure grade (purity > 99.999%) is needed. At present, the most mature technology for hydrogen purification to such a grade is based on Pd or Pd-Ag alloy membranes [1]. In this hydrogen purification system, hydrogen molecules are ionized catalytically to obtain H^+ ions, on one of the surfaces of the membrane. H^+ ions solubilize in the material and, due to the gradient of pressure and concentration, they diffuse through the membrane towards the other surface, where they recombine to form ultrapure H_2 molecules. Metallic alloys, both crystalline and amorphous, display high selectivity for hydrogen and this characteristic allows to obtain the ultrapure grade of the hydrogen gas permeated through the metallic membranes [1].

Despite the very good performances of Pd and Pd-Ag alloy membranes, it must be considered that Pd is an expensive (about $24,000 USD/kg) and strategic metal. Moreover, in some conditions Pd

can suffer from embrittlement. Therefore, a large effort in the research of alternative membranes have been conducted in the last years.

Separation of gases by means of polymeric membranes is already used in industrial processes, such as the production of technical-grade nitrogen, the hydrogen separation in refineries and the petrochemical industry, and the separation of CO_2 from CH_4 or N_2 [2–4]. However, this type of membrane, which is relatively cheap, can found applications only when gas separation can occur in the temperature range below 100 °C. Moreover, their selectivity is relatively low (not exceeding 100 [3]) and, therefore, they can be used only when the purity of the permeated gas is not a primary concern [1]. Polymeric membranes suffer from swelling and poisoning [1]. Another concern about polymer membranes is the need to recover the toxic by-products for their production [5].

Metallic membranes based on chemical elements different from Pd can be a valid alternative, as they show high selectivity (>1000) and an operational temperature range between 300 °C and 600 °C [1]. Indeed, some metals show a permeability comparable to, or even higher than, Pd [6]. Many of them, such as Ni, Co, Nb, and Zr cost in the range of $5–40 USD/kg and, therefore, are considered as possible alternatives to palladium. However, crystalline materials usually become brittle when they are hydrogenated. In this framework, in the last years, an important effort has been devoted to the study of metallic amorphous membranes [7,8]. Indeed, the pioneering research of Hara et al. [9–11] reported that the hydrogen permeability of $Ni_{64}Zr_{36}$ is of the order of 10^{-9} mol m^{-1}·s^{-1}·Pa$^{-0.5}$. These amorphous membranes do not become brittle and are stable at least up to 350 °C [9–11]. Since these initial studies about amorphous membranes for hydrogen purifications, many chemical compositions have been investigated (see [1,8]). The review of Ockwig and Nenoff [1] reported different types of hydrogen separation membranes and reported hydrogen permeability of Ni-Al, V-Al, V-Ni-Al, Nb-Mo, Nb-Pd, Nb-Ti-Ni, V-Ti, V-Co, Zr-Ti-Ni, and other alloys, in the temperature range between 475 K and 673 K and of V-Cr-Ti from 793 K to 923 K. Ni-Nb-Zr alloys are the most widely studied system from the perspective of hydrogen separation. In some cases, doping with other alloying elements, such as Ta, Co, Hf, Ti, Ta, Sn, Si, Pd, Cu, Co, and Al, has been investigated [8,12]. In general, the addition of Nb to Ni-Zr alloys, similar to those initially proposed by Hara et al. [9–11], produces beneficial effects: it increases the crystallization temperature and the fracture strength and reduces the hydrogen embrittlement [13]. Moreover, it has been shown that some Ni-Nb-Zr membranes (such as $Ni_{30}Nb_{40}Zr_{30}$, $Ni_{60}Nb_{30}Ti_{10}$, and the presently-investigated $(Ni_{0.6}Nb_{0.4})_{100-x}Zr_x$ membranes) display a hydrogen permeability higher than that of $Ni_{64}Zr_{36}$, of the order of 10^{-8} mol·m^{-1}·s^{-1}·Pa$^{-0.5}$, a value comparable to, or even higher than, that of the Pd-based alloys [8].

One of the main concerns about the amorphous membranes is their propensity to crystallize when heated to temperatures close to those ones (400–450 °C) needed for hydrogen purification. Indeed, crystalline phases are usually more brittle than the amorphous ones. For this reason, a preliminary investigation of the crystallization process is needed for each new composition.

Although the permeation rates of the membranes are very important, one should consider that solubility and diffusion rates are strictly mathematically linked. If one assumes the diffusion coefficient to be constant, the relationship between the diffusion coefficient, D, the permeation coefficient, P, and the solubility coefficient, S, simplifies to P = D × S. Moreover, the hydrogen flux through a membrane is linked to the shape of the pressure composition isothermal curves of the material [14]. Therefore, a deep knowledge of the hydrogen solubility of membranes is strategic to characterize their potential applicative use. The mechanical stability of amorphous membranes during operation at high temperatures is another important concern in view of their application. In fact, the sample should not become brittle or present faults due to thermal treatments and/or hydrogenation. Finally, the evolution of the physical properties of membranes with increasing temperature in the presence of hydrogen should also be considered. In fact, quite recently it has been reported the occurrence of an abrupt expansion induced by hydrogenation of the amorphous structure of a $Ni_{32}Nb_{28}Zr_{30}Cu_{10}$ membrane between 240 and 300 °C. Correspondingly, also the sorption properties are drastically changed and the solubility strongly decreases [15].

In this work, we report some new investigations of the physical properties of amorphous membranes based on Ni, Nb, and Zr metals. In particular, the dependence of the crystallization temperature and of the hydrogen solubility at 400 °C on the Zr content in $(Ni_{0.6}Nb_{0.4})_{100-x}Zr_x$ (x = 0, 10, 20, and 30) are measured. Upon partial replacement of Nb by Ta, no major changes in the crystallization process or the sorption properties are observed. Moreover, we compare the solubility of amorphous and crystallized $(Ni_{0.6}Nb_{0.4})_{70}Zr_{30}$. The crystallized samples are not useful for applications, because they pulverized upon hydrogenation, but, to the best of our knowledge, their solubility properties have not been measured until now. Finally, for the first time, the sorption of a boron containing Ni-Nb-Zr membrane is studied as a function of temperature. The motivation behind the choice of doping with B resides in the recent observation [16] that the addition of 1–5 at% of B to amorphous $Zr_{66.7-x}Ni_{33.3}$ membranes increases their thermal stability, the microhardness, and resistance to corrosion. Moreover, boron can form a large variety of complexes with metals [17] and, therefore, it is expected to increase the hydrogen solubility.

2. Results and Discussion

2.1. Changes of the Physical Properties as a Function of the Zr Content

The occurrence of crystallization upon heating is observed from differential thermal analysis (DTA) measurements. Figure 1 shows DTA curves of various samples of $(Ni_{0.6}Nb_{0.4})_{100-x}Zr_x$ with different concentrations of Zr (x = 0, 10, 20, and 30). In order to properly compare the effects of Zr concentration, the temperature scanning rate is fixed at 10 °C/min. All samples display exothermic peaks above 500 °C, corresponding to the crystallization process. Consistently with previous partial measurements, it is well evident that the peaks shift to lower temperature as the Zr content increases [18]. A similar decrease in the crystallization temperature with increasing Zr content was reported for Ni-Nb-Zr alloys, with the addition of Co [19]. Table 1 shows the temperature at which crystallization starts, $T_{c,onset}$, defined as the temperature at which one observes the deviation from the linear background displayed by the DTA curves at low temperature.
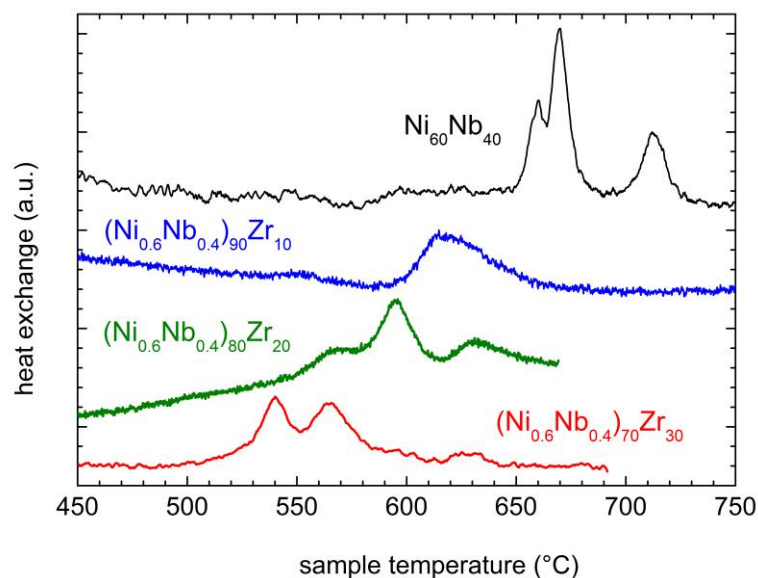

Figure 1. DTA curves of samples $(Ni_{0.6}Nb_{0.4})_{100-x}Zr_x$ for x = 0, 10, 20, and 30, measured with a temperature rate of 10 °C/min.

Table 1. Onset temperature for crystallization, $T_{c,onset}$, in $(Ni_{0.6}Nb_{0.4})_{100-x}Zr_x$ membranes as a function of Zr content, x.

X	$T_{c,onset}$ (°C)
0	648 ± 2
10	591 ± 3
20	547 ± 3
30	506 ± 2

Figure 1 also shows that only in the case of $(Ni_{0.6}Nb_{0.4})_{90}Zr_{10}$ the crystallization seems to occur in a single step, giving rise to a single peak in the DTA measurements. For all other samples, crystallization is present as a multistep process, corresponding to three peaks in the DTA curves.

Crystallization of the amorphous membranes is usually a thermally-activated process, as the DTA peaks shift to higher temperatures when measured with higher temperature rates [18]. The activation energy of the crystallization, E_a, occurring in the samples with x = 20 and 30 have been already reported [18]: E_a is ~549 kJ/mol for x = 20 and ~542 kJ/mol for x = 30. In the present work, we extend such a study to the case x = 10. To determine the activation energy, DTA curves are obtained at various scanning rates (Figure 2). It is quite evident that the peaks shift to higher T as the scan rates increase. The inset of Figure 2 shows the Kissinger plot for the crystallization process and the best-fit line. The activation energy is obtained from the slope of the linear fit, which in the present case is 640 ± 60 kJ/mol. This value, obtained for x = 10, is higher than those reported in the case of samples with x = 20 and 30 [18].
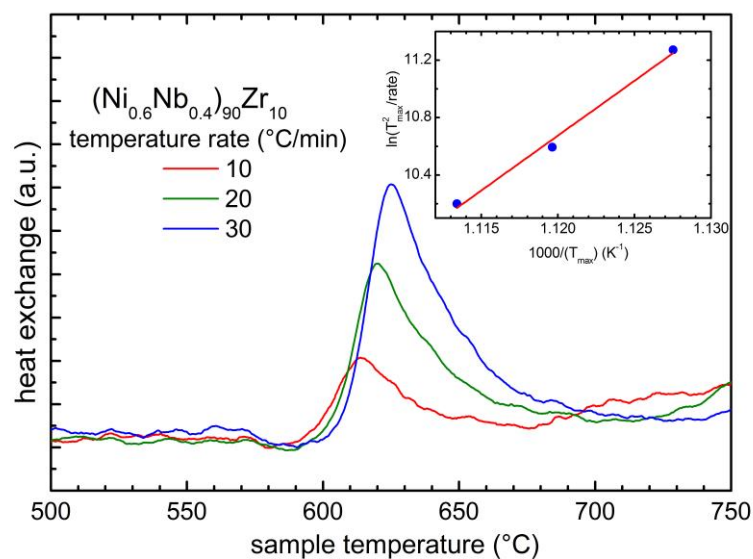

Figure 2. DTA curves of sample $(Ni_{0.6}Nb_{0.4})_{90}Zr_{10}$, measured at various temperature rates. The inset shows the Kissinger plot for the crystallization peak and the best fit line.

Figure 3 shows the comparison of the solubility measured at 400 °C for the three membranes with x = 10, 20, and 30, and of one ribbon with the composition $(Ni_{0.6}Nb_{0.3}Ta_{0.1})_{70}Zr_{30}$. The last three compounds were also investigated as a function of temperature in [20]. For x = 10, investigated here for the first time, the kinetics of hydrogen absorption is so slow that we could not measure pressure-composition isotherm at temperatures lower than 400 °C (it took almost one day to observe pressure equilibration for each experimental point reported in Figure 3). The hydrogen solubility reported in Figure 3 and subsequent ones is expressed as H/M, i.e., the number of hydrogen atoms per atom of metal of the alloy (see section Materials and Methods for definition). It is quite evident from Figure 3 that the hydrogen solubility increases with increasing Zr content; for a pressure of ~7 bar,

which is the maximum applied pressure in the present study, we obtained a value of H/M equal to ~0.16 for x = 10, ~0.24 for x = 20 and ~0.36 for x = 30.
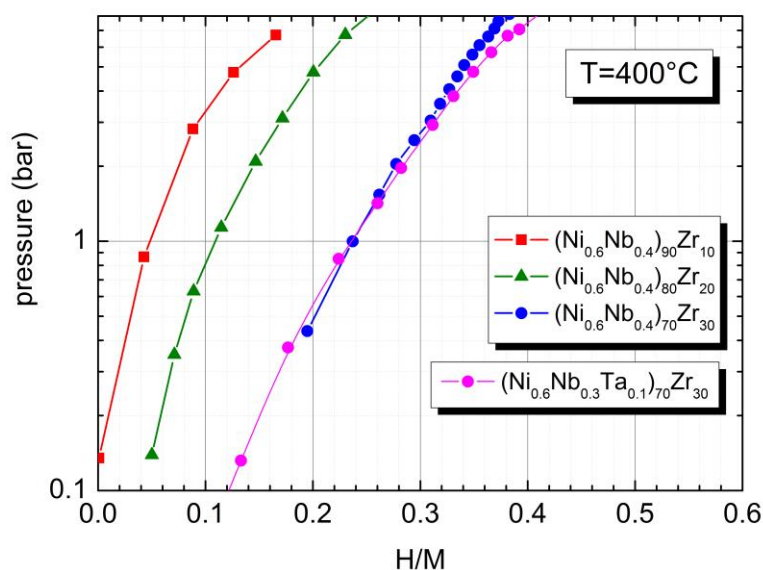

Figure 3. Pressure-composition isotherms measured at 400 °C for $(Ni_{0.6}Nb_{0.4})_{100-x}Zr_x$ samples as a function of the Zr content. For comparison, also the isotherm of sample $(Ni_{0.6}Nb_{0.3}Ta_{0.1})_{70}Zr_{30}$ is reported.

Conversely, the Ta content in the compounds seems to play only a marginal effect on the absorption properties, although substitution of Nb with Ta causes a slight increase of the crystallization temperature and does not vary the permeability significantly [21]. In Figure 3, one can observe that the pressure-composition isotherms of $(Ni_{0.6}Nb_{0.4})_{70}Zr_{30}$ and $(Ni_{0.6}Nb_{0.3}Ta_{0.1})_{70}Zr_{30}$ are close one to the other. Further details on solubility as a function of temperature of $(Ni_{0.6}Nb_{0.4-y}Ta_y)_{100-x}Zr_x$ membranes with y = 0, 0.1 and x = 20, 30 can be found in [20].

2.2. Hydrogen Sorption Properties in the Amorphous and in the Crystalline State

To the best of our knowledge, a comparison of the solubility properties of amorphous and crystalline materials is not available. For this reason, the pressure composition isotherms of amorphous and crystalline $(Ni_{0.6}Nb_{0.4})_{70}Zr_{30}$ are here measured. Figure 4 displays both the absorption and desorption isotherms of $(Ni_{0.6}Nb_{0.4})_{70}Zr_{30}$, measured at 300 °C and 350 °C for the amorphous membrane and at 280 °C and 350 °C for the crystalline sample. The latter one was obtained as reported in section Materials and Methods. In the amorphous sample, one observes that the solubility decreases at higher temperature, while the hydrogen concentration at fixed temperature smoothly increases as pressure increases. Additionally, the desorption curves are smooth and do not present pressure plateaus. However, it is worth noting the occurrence of a clear hysteresis between the absorption and desorption curves. The occurrence of hysteresis during hydrogenation/dehydrogenation is a well-known property of metal powders, discussed in previous literature [22]. Due to the fast kinetics, it was possible to measure an entire absorption/desorption isotherm in 1 day for the amorphous sample.

The crystallized membrane isotherms show sorption curves with a shape different from that of the amorphous sample: the crystallized sample displays the presence of a "slopey" pressure plateau, as, indeed, expected for crystalline compounds [23]. Additionally, the crystalline membranes show a hysteresis between absorption and desorption. The kinetics of the crystallized sample is extremely slow when dealing with the low pressure part of the curve: it took about 10 days to measure the absorption/desorption curve for P < 5 bar, whereas the phase that forms at P ~6 bar for T = 280 °C is able to absorb/desorb in a few minutes, possibly due to the formation of new sites due to lattice

expansion. However, the amount of hydrogen stored in that phase is quite low ($\Delta H/M \sim 0.06$, from the width of the pressure plateau around H/M ~0.34 in Figure 4). To measure the two isotherms of the crystallized sample, it took one month and a half. Such a long time of acquisition limited the possibility to measure crystallized samples with different elemental composition.
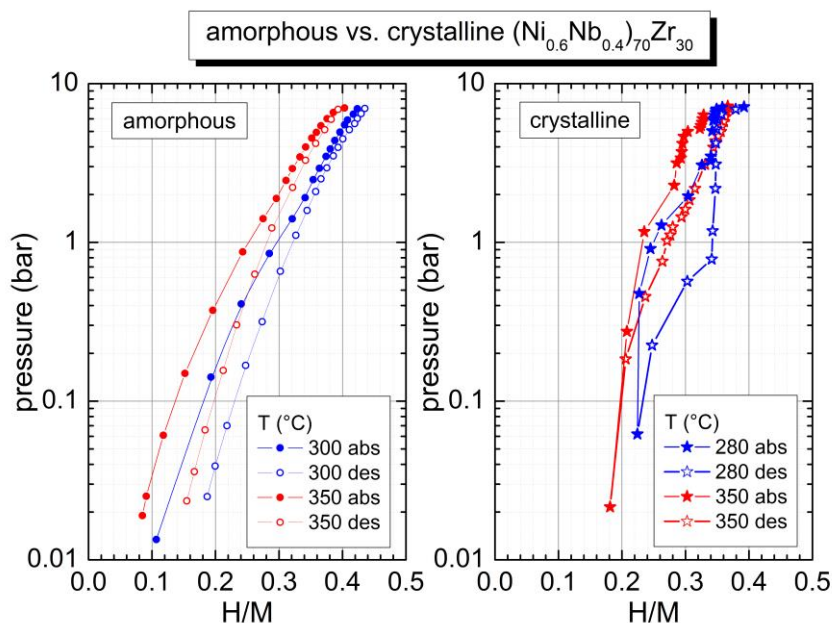

Figure 4. Pressure-composition isotherms at two temperatures for amorphous and crystalline $(Ni_{0.6}Nb_{0.4})_{70}Zr_{30}$.

Another aspect that needs to be highlighted is the fact that in the crystalline material one observes a near vertical trend of the pressure-composition isotherm for low H/M values, while in the amorphous ribbons the tangent of the curve forms an acute angle with the horizontal axis. Such a behavior indicates that it is more difficult to remove hydrogen from the crystalline material than from the amorphous sample, i.e., one should reduce the pressure values to a much lower values in the crystalline membrane than in amorphous samples to have a complete dehydrogenation, starting from the same initial pressure value.

2.3. Physical Properties of a Boron Containing Sample

In this study, the influence of the addition of a small concentration of boron in a Ni-Nb-Zr ribbon is investigated, studying a membrane with composition $(Ni_{0.42}Nb_{0.28}Zr_{0.30})_{98}B_2$. The crystallization process was firstly investigated, in order to check that the addition of boron did not significantly decrease the crystallization temperature with respect to the $(Ni_{0.6}Nb_{0.4})_{70}Zr_{30}$ sample. Figure 5 shows the DTA curves of the boron containing membrane, measured at various temperature scanning rates. An exothermic peak, corresponding to the crystallization, is visible above 500 °C, possibly followed at higher temperatures by a broader peak. For the curve measured at 10 °C/min, the departure from a linear background is revealed at ~510 ± 3 °C, a value close to that (506 ± 2 °C) obtained for $(Ni_{0.6}Nb_{0.4})_{70}Zr_{30}$ and reported in Table 1. In view of these results, we can assert that the addition of boron does not significantly affect the crystallization temperature and the thermal stability of the membrane. However, the boron-containing membrane displays only one well-defined peak in the DTA curve, while other materials, without B, show multiple peaks (see Figure 1). Additional studies are needed in order to ascertain the origin of such an effect.
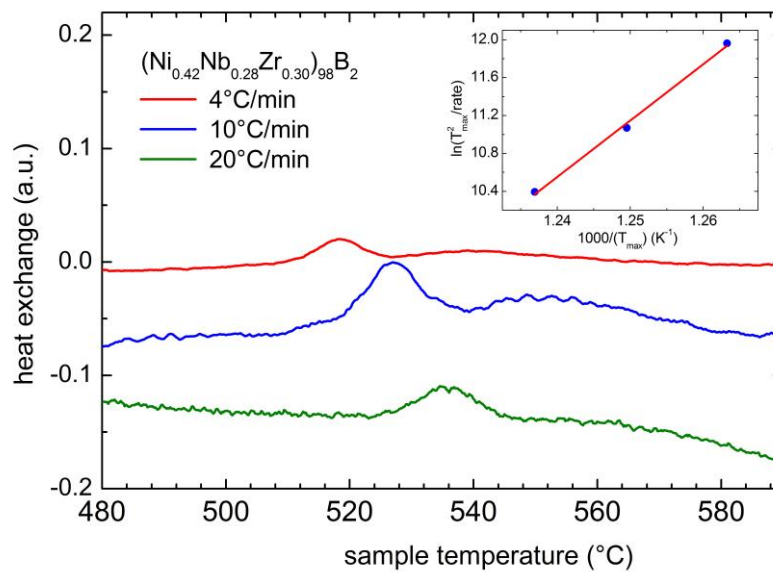
Figure 5. DTA measurements of $(Ni_{0.42}Nb_{0.28}Zr_{0.30})_{98}B_2$ measured at various temperature rates. The inset shows the Kissinger plot for the crystallization peak and the best fit line.

The activation energy, E_a, of the crystallization process is obtained from the Kissinger plot, reported in the inset of Figure 5. For the boron containing sample $E_a = 500 \pm 30$ kJ/mol. This value is lower than that obtained for $(Ni_{0.6}Nb_{0.4})_{70}Zr_{30}$, E_a ~540 kJ/mol.

On the other hand, the sorption properties of the sample containing boron are modified with respect to the corresponding membranes without boron. Figure 6 displays the absorption pressure-composition isotherms of $(Ni_{0.42}Nb_{0.28}Zr_{0.30})_{98}B_2$ measured between 440 °C and 485 °C. Indeed, as the kinetics of the boron-containing membrane is slow below 420 °C, we could not obtain absorption curves below 440 °C.
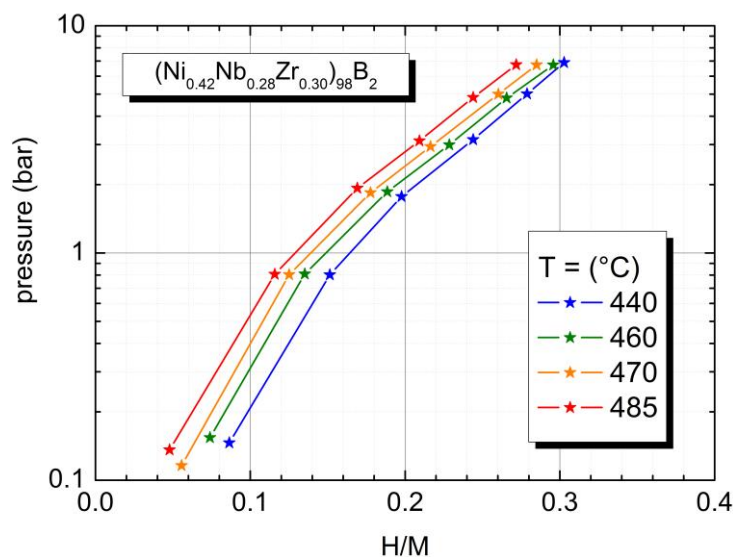

Figure 6. Pressure-composition isotherms of sample $(Ni_{0.42}Nb_{0.28}Zr_{0.30})_{98}B_2$ measured between 440 °C and 485 °C.

The hydrogen solubility decreases as temperature increases, as already reported for other Ni-Nb-Zr amorphous membranes [15,20]. Indeed, the maximum concentration of hydrogen obtained

for p ~7 bar decreases from ~0.31 H/M at T = 440 °C to ~0.27 H/M at T = 485 °C. Moreover, the entire absorption curve is displaced towards lower solubility values as temperature increases.

From the pressure-composition isotherms, one can obtain the value of the hydrogenation enthalpy using the so called van't Hoff plot. In crystalline materials, pressure plateau are observed in isotherms, at p^*, and the van't Hoff plot reports $\ln(p^*)$ vs. $1/T$; the slope of the best fit lines provides the hydrogenation enthalpy, ΔH_{hyd}. In amorphous materials, no pressure plateau can be observed. However, one can still construct a van't Hoff plot reporting $\ln(p)$ vs. $1/T$, where p is the pressure at a fixed value of H/M at the various temperatures. Additionally, in this case, one can estimate the hydrogenation enthalpy, ΔH_{hyd}, from the slope of the plot [24].

Figure 7 shows the van't Hoff plot of the boron containing membrane, calculated at various H/M ratios. In order to construct such a graph, the experimental pressure-composition isotherms were interpolated by means of beta splines, thanks to a program implemented with the Labview (National Instruments, Austin, TX, USA) routines. Table 2 reports the values of the hydrogenation enthalpy, calculated from the slope of the lines of Figure 7. A decrease of the hydrogenation enthalpy as the hydrogen concentration increases from 0.10 to 0.20 can be noted (see Table 2). Indeed, ΔH_{hyd} passes from 89 ± 9 kJ/mol H_2 at H/M = 0.10 to 43 ± 3 kJ/mol H_2 at H/M = 0.20. The decrease of the hydrogenation enthalpy with increasing hydrogen content was already reported for $(Ni_{0.6}Nb_{0.4-y}Ta_y)_{100-x}Zr_x$ with y = 0, 0.1 and x = 20, 30 [20], and for $Ni_{32}Nb_{28}Zr_{30}Cu_{10}$ [15]. As a comparison, in $(Ni_{0.6}Nb_{0.4})_{70}Zr_{30}$ the hydrogenation enthalpy varies from ~41 kJ/mol for H/M = 0.34 to ~33 kJ/mol for H/M = 0.42; in $(Ni_{0.6}Nb_{0.4})_{80}Zr_{20}$, ΔH_{hyd} decreases from ~14 kJ/mol at H/M = 0.10 to ~8 kJ/mol at H/M = 0.16 [20]. In $(Ni_{0.6}Nb_{0.4-y}Ta_y)_{100-x}Zr_x$ the decrease of ΔH as H/M increases was attributed to the progressive occupation of interstitial sites available for hydrogen trapping during the absorption process [20]. In fact, at the beginning of the process, the deepest energy levels become occupied, leaving shallower energy levels empty. The former become occupied only at higher hydrogen concentrations and, therefore, the hydrogenation enthalpy decreases as H/M increases [20]. Indeed, Jayalakshmi et al. [25] investigated the thermal desorption process of some Ni-Nb-Zr-Ta amorphous ribbons by means of thermal desorption spectroscopy. These authors [25] linked the dehydrogenation temperature to the energy of the sites occupied by hydrogen atoms: the strongly bonded interstitial sites desorbed at higher temperature than the weakly bonded sites. For samples containing less than 40 at% H, the dehydrogenation occurred above 500 °C, while at higher hydrogen content dehydrogenation started already at 200 °C. These facts suggest that at lower H/M the deeper energy interstitial sites are occupied by hydrogen [25], while at higher H/M also the shallower energy levels become populated. The absorption data presently reported [25] are consistent with this picture: at higher H/M the hydrogenation enthalpy decreases because the absorption involves the shallower energy sites. In the presently-investigated $(Ni_{0.42}Nb_{0.28}Zr_{0.30})_{98}B_2$ membrane, no change of the hydrogenation enthalpy is observed above H/M = 0.20.

Finally, we want to point out that, despite the high temperatures reached during the sorption measurements, the boron-containing membranes used for the Sieverts measurements maintained their shape and did not pulverize after the hydrogenations and thermal cycles (in total, nine cycles, including the ones used for activating the membranes).

Table 3 reports a summary of the elemental composition, the crystallization temperature T_C (defined as the maximum of the first peak in DTA measurements conducted with a temperature rate of 10 °C/min), solubility at T = 400 °C and p = 7 bar and dehydrogenation enthalpy of the investigated membranes.
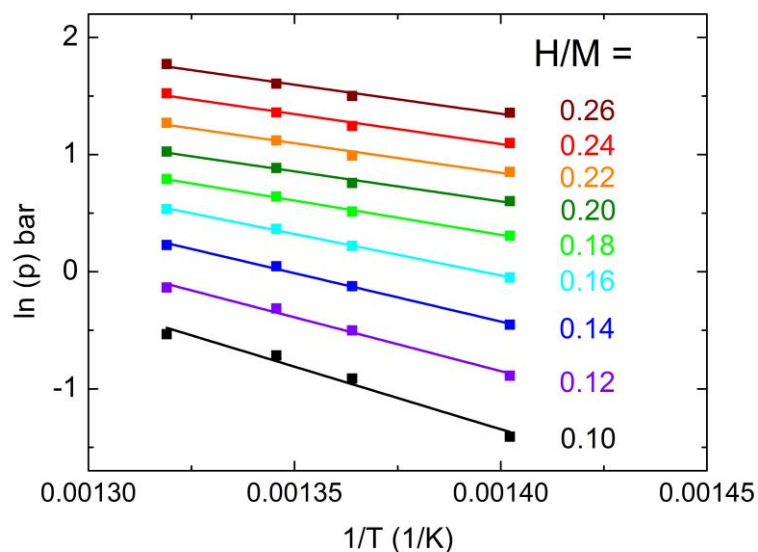
Figure 7. Van't Hoff plot for the $(Ni_{0.42}Nb_{0.28}Zr_{0.30})_{98}B_2$ membrane calculated at different H/M ratios and best fit lines.

Table 2. Hydrogenation enthalpy, ΔH_{hyd}, calculated for $(Ni_{0.42}Nb_{0.28}Zr_{0.30})_{98}B_2$ at various H/M values.

H/M	ΔH_{hyd} (kJ/mol)
0.10	89 ± 9
0.12	76 ± 5
0.14	69 ± 3
0.16	59 ± 3
0.18	49 ± 2
0.20	43 ± 3
0.22	43 ± 3
0.24	43 ± 3
0.26	43 ± 3

Table 3. Elemental composition, crystallization temperature T_C (defined as the maximum of the first peak in DTA measurements conducted with a temperature rate of 10 °C/min), solubility at T = 400 °C and p = 7 bar and dehydrogenation enthalpy of the investigated membranes.

Elemental Composition	Tc (°C)	Solubility (H/M)	ΔH (kJ/mol)
$(Ni_{0.6}Nb_{0.4})_{90}Zr_{10}$	615	0.16	–
$(Ni_{0.6}Nb_{0.4})_{80}Zr_{20}$	567	0.24	14 (H/M = 0.10) [20] 8 (H/M = 0.16) [20]
$(Ni_{0.6}Nb_{0.4})_{70}Zr_{30}$	540	0.36	41 (H/M = 0.34) [20] 33 (H/M = 0.42) [20]
$(Ni_{0.42}Nb_{0.28}Zr_{0.30})_{98}B_2$	526	0.31 (T = 440 °C)	89 (H/M = 0.10) 43 (H/M = 0.20)

3. Materials and Methods

Buttons of the investigated alloys were obtained by arc melting the pure elements (Ni, Nb, Zr, Ta, B) in an argon atmosphere at AMES Laboratory, Ames, Iowa, USA, in the proper weight proportions. The elemental composition of the alloys, as reported in the whole paper, corresponds to the initial concentration of elements used for the preparation of the materials. For each composition investigated

in the paper, one ingot of crystalline material was produced. These initial alloys are crystalline and need further processing to become amorphous. Indeed, subsequently, the buttons were used to fabricate the amorphous membranes by means of a melt spinning apparatus at the CSIRO laboratory, Brisbane, Australia [26]. In the melt spinning apparatus, the alloys are melted and are, subsequently, extruded onto a copper wheel, cooled by water. The rapid solidification, occurring with a temperature rate of the order of $\Delta T/\Delta t \sim 10^5 \; ^\circ C \cdot s^{-1}$, produces an amorphous state for the alloys. These amorphous ribbons have typical thickness of ~30–70 μm and a width of ~30 mm [26], and are those investigated throughout the paper. Only in the case of a specimen of $(Ni_{0.6}Nb_{0.4})_{70}Zr_{30}$, recrystallization was obtained by means of a thermal treatment of an amorphous sample in a thermogravimetric apparatus, a Setaram Sensys Evolution 1200 TGA system (Setaram Instrumentation, Caluire, France), heating to 700 $^\circ$C in a pure argon atmosphere (60 mL/min), using a temperature scanning rate of 10 $^\circ$C/min. Previous X-Ray Diffraction measurements indicated that this treatment induces the occurrence of crystallization and Bragg peaks due to a $Ni_{48}Zr_{52}$ phase and possibly to a $Ni_{10}Zr_7$ phase can be detected [27].

DTA curves were measured by means of a Setaram Sensys Evolution 1200 TGA system [28] under a high purity argon flux (60 mL/min). For each temperature scan, a piece of a sample with a mass of ~10 mg was measured. For each specimen, acquisitions with various temperature rates, ranging between 4 $^\circ$C and 30 $^\circ$C/min, were used in order to calculate the activation energy of the crystallization process.

Pressure-composition isotherms were recorded by a homemade Sieverts apparatus described elsewhere [27,29]. For each sample, measurements were conducted with a mass of 300–500 mg. In all graphs of the pressure-composition isotherms, pressure is referred to the molecular hydrogen gas in equilibrium with the solid, while the concentration is expressed as H/M, i.e., the number of hydrogen atoms per atom of metal composing the dehydrogenated alloy. During the acquisition of pressure-composition isotherms, the variation of the number of gaseous molecular hydrogen due to a change in the applied pressure is measured, $\Delta n(H_2)$. Consequently the number of moles of atomic hydrogen absorbed or desorbed from the solid can be calculated as $\Delta n(H) = 2 \cdot \Delta n(H_2)$. The number of moles of the dehydrogenated alloy, n_{alloy}, is obtained by the measure of the initial mass of the sample (m_{alloy}): $n_{alloy} = m_{alloy}/M_{alloy}$, where M_{alloy} is the mass of a formula unit. Consequently, the variation of the number of hydrogen atoms per metal atom can be calculated as $\Delta n(H)/n_{alloy} = 2 \cdot \Delta n(H_2) \cdot M_{alloy}/m_{alloy}$. Adding contributions due to subsequent change of pressure, one can easily obtain $n(H)/n_{alloy}$, which is the ratio of the number of moles of atomic hydrogen and the number of moles of metal at a certain pressure and temperature or, equivalently, the number of hydrogen atoms per metal atom, which is usually called H/M [30].

4. Conclusions

In this work we investigated a series of amorphous membranes based on Ni, Nb, and Zr metals. In $(Ni_{0.6}Nb_{0.4})_{100-x}Zr_x$ the onset crystallization temperature decreases from ~590 $^\circ$C for x = 10 to ~510 $^\circ$C for x = 30. Concomitantly, the activation energy of the crystallization decreases from ~640 kJ/mol for x = 10 to ~550 kJ/mol for x = 30. The hydrogen solubility measured at 400 $^\circ$C increases for increasing Zr content.

A hysteresis between the absorption and desorption pressure-composition isotherms is observed both in amorphous and in crystallized $(Ni_{0.6}Nb_{0.4})_{70}Zr_{30}$. However, the crystalline sample shows multiple pressure plateaus, due to the hydrogenation of various crystalline phases. A slow kinetics of the sorption processes in the crystalline state is observed. Conversely, in the amorphous state, a smooth behavior of the p-c isotherms is visible and the sorption kinetics are much faster.

Finally, the addition of a small amount of boron to $(Ni_{0.6}Nb_{0.4})_{70}Zr_{30}$ is investigated. The crystallization temperature is not significantly affected, while the activation energy of the crystallization process decreases. The sorption properties are measured above 440 $^\circ$C, showing a good hydrogen solubility. The hydrogenation enthalpy passes from 89 ± 9 kJ/mol H_2 at H/M = 0.10 to 43 ± 3 kJ/mol H_2 at H/M = 0.20. This behavior, similar to that observed in similar membranes,

is attributed to the fact that, at the beginning of hydrogenation, the lowest energy sites become populated, while lately only shallower energy levels become occupied, with a consequent change in the energy requested for hydrogenation. It should be noted that the boron-containing membrane does not pulverize even after repeated thermal cycles and hydrogenation processes up to 485 °C and 7 bar.

Author Contributions: Michael Dolan produced the melt spun membranes; Oriele Palumbo and Francesco Trequattrini performed the DTA measurements and analysis; Narendra Pal, Madhura Hulyakar, Suchismita Sarker and Dhanesh Chandra conducted preliminar solubility measurements; Annalisa Paolone performed the Sieverts hydrogen sorption measurements and analysis; Dhanesh Chandra and Annalisa Paolone wrote the paper; all authors discussed the data and shared the conclusions.

Conflicts of Interest: The authors declare no conflict of interest.

References

1. Ockwig, N.W.; Nenoff, T.M. Membranes for Hydrogen Separation. *Chem. Rev.* **2007**, *107*, 4078–4110. [CrossRef] [PubMed]

2. Budd, P.M.; McKeown, N.B. Highly permeable polymers for gas separation membranes. *Polym. Chem.* **2010**, *1*, 63–68. [CrossRef]

3. Yampolskii, Y. Polymer Gas Separation Membranes. *Macromolecule* **2012**, *45*, 3298–3311. [CrossRef]

4. Sanders, D.F.; Smith, Z.P.; Guo, R.; Robeson, L.M.; McGrath, J.E.; Paul, D.R.; Freeman, B.D. Energy-efficient polymer gas separation membranes for a sustainable future: A review. *Polymer* **2013**, *54*, 4729–4761. [CrossRef]

5. Razali, M.; Kim, J.F.; Attfield, M.; Budd, P.M.; Drioli, E.; Lee, Y.M.; Szekely, G. Sustainable wastewater treatment and recycling in membrane manufacturing. *Green Chem.* **2015**, *17*, 5196–5205. [CrossRef]

6. Steward, S.A. *Review of Hydrogen Isotope Permeability through Metals*; U.S. National Laboratory Report: UCRL-53441; Lawrence Livermore National Lab.: Livermore, CA, USA, 1983.

7. Dolan, M.D.; Dave, N.C.; Ilyushechkin, A.Y.; Morpeth, L.D.; McLennan, K.G. Composition and operation of hydrogen-selective amorphous alloy membrane. *J. Membr. Sci.* **2006**, *285*, 30–55. [CrossRef]

8. Sarker, S.; Chandra, D.; Hirscher, M.; Dolan, M.; Isheim, D.; Wermer, J.; Viano, D.; Baricco, M.; Udovic, T.J.; Grant, D.; et al. Developments in the Ni-Nb-Zr Amorphous Alloy Membranes. *Appl. Phys. A* **2016**, *122*, 168:1–168:9. [CrossRef]

9. Hara, S.; Hatakeyma, N.; Itoh, N.; Kimura, H.-M.; Inoue, A. Hydrogen permeation through amorphous $Zr_{36-x}Hf_xNi_{64}$ alloy membranes. *J. Membr. Sci.* **2003**, *211*, 149–156. [CrossRef]

10. Hara, S.; Sakaki, K.; Itoh, N.; Kimura, H.-M.; Asami, K.; Inoue, A. An amorphous alloy membrane without noble metals for gaseous hydrogen separation. *J. Membr. Sci.* **2000**, *164*, 289–294. [CrossRef]

11. Hara, S.; Hatakeyma, N.; Itoh, N.; Kimura, H.-M.; Inoue, A. Hydrogen permeation through palladium-coated amorphous Zr-M-Ni (M = Ti, Hf) alloy membranes. *Desalination* **2002**, *144*, 115–120. [CrossRef]

12. Yamaura, S.-I.; Simpo, Y.; Okouchi, H.; Nishida, M.; Kajita, O.; Inoue, A. The Effect of Additional Elements on Hydrogen permeation Properties of Melt-spun Ni-Nb-Zr amorphous alloys. *Mater. Trans.* **2004**, *45*, 330–333. [CrossRef]

13. Kimura, H.; Inoue, A.; Yamaura, S.-I.; Sasamori, K.; Nishida, M.; Shinpo, Y.; Okouchi, H. Thermal stability and mechanical properties of glassy and amorphous Ni-Nb-Zr alloys produced by rapid solidification. *Mater. Trans. JIM* **2003**, *44*, 1167–1171. [CrossRef]

14. Suzuki, A.; Yukawa, H.; Nambu, T.; Matsumoto, Y.; Murata, Y. Consistent description of hydrogen permeability through metal membrane based on hydrogen chemical potential. *Int. J. Hydrogen Energ.* **2014**, *39*, 7919–7924. [CrossRef]

15. Palumbo, O.; Trequattrini, F.; Hulyalkar, M.; Sarker, S.; Pal, N.; Chandra, D.; Flanagan, T.; Dolan, M.; Paolone, A. Hydrogen induced abrupt structural expansion at high temperatures of a $Ni_{32}Nb_{28}Zr_{30}Cu_{10}$ membrane for H_2 purification. *Membranes* **2016**, *6*, 48. [CrossRef] [PubMed]

16. Xu, J.; Niu, J.; Zhang, Z.; Ge, W.; Shang, C.; Wang, Y. Effects of B addition on glass formation, mechanical properties and corrosion resistance of the $Zr_{66.7-x}Ni_{33.3}B_x$ (x = 0, 1, 3, and 5 at%) metallic glasses. *JOM* **2016**, *68*, 682–691. [CrossRef]

17. Li, H.-W.; Yan, Y.; Orimo, S.-I.; Züttel, A.; Jensen, C.M. Recent Progress in Metal Borohydrides for Hydrogen Storage. *Energies* **2011**, *4*, 185–214. [CrossRef]

18. Kim, S.-M.; Chandra, D.; Pal, N.K.; Dolan, M.D.; Chien, W.-M.; Talekar, A.; Lamb, J.; Paglieri, S.N.; Flanagan, T.B. Hydrogen permeability and crystallization kinetics in amorphous Ni-Nb-Zr alloys. *Int. J. Hydrogen Energ.* **2012**, *37*, 3904–3913. [CrossRef]

19. Shimpo, Y.; Yamaura, S.I.; Nishida, M.; Kimura, H.; Inoue, A. Development of melt-spun Ni–Nb–Zr–Co amorphous alloy for high-performance hydrogen separating membrane. *J. Membr. Sci.* **2006**, *286*, 170–173. [CrossRef]

20. Palumbo, O.; Trequattrini, F.; Pal, N.; Hulyalkar, M.; Sarker, S.; Chandra, D.; Flanagan, T.; Dolan, M.; Paolone, A. Hydrogen absorption properties of amorphous $(Ni_{0.6}Nb_{0.4-y}Ta_y)_{100-x}Zr_x$ membranes. *Prog. Nat. Sci.* **2017**. [CrossRef]

21. Qiang, J.B.; Zhang, W.; Yamaura, S.; Inoue, A. Thermal Stability and Hydrogen Permeation of $Ni_{42}Zr_{30}Nb_{28-x}Ta_x$ Amorphous Alloys. *Mater. Trans.* **2009**, *50*, 1236–1239. [CrossRef]

22. Rabkin, E.; Skripnyuk, V.N. On pressure hysteresis during hydrogenation of metallic powders. *Scripta Mater.* **2003**, *49*, 477–483. [CrossRef]

23. Kirchheim, R.; Sommer, F.; Schluckebier, G. Hydrogen in amorphous metal I. *Acta Metall.* **1982**, *30*, 1069–1078. [CrossRef]

24. Karger, B.L.; Snyder, L.R.; Horvath, C. *An Introduction to Separation Science*; Wiley: New York, NY, USA, 1973.

25. Jayalakshmi, S.; Choi, Y.G.; Kim, Y.C.; Kim, Y.B.; Fleury, E. Hydrogenation properties of Ni-Nb-Zr–Ta amorphous ribbons. *Intermetallics* **2010**, *18*, 1988–1993. [CrossRef]

26. Paglieri, S.N.; Pal, N.K.; Dolan, M.D.; Kim, S.-M.; Chien, W.-M.; Lamb, J.; Chandra, D.; Hubbard, K.M.; Moore, D.P. Hydrogen permeability, thermal stability and hydrogen embrittlement of Ni-Nb-Zr and Ni-Nb-Ta-Zr amorphous alloy membranes. *J. Membr. Sci.* **2011**, *378*, 42–50. [CrossRef]

27. Palumbo, O.; Brutti, S.; Trequattrini, F.; Sarker, S.; Dolan, M.; Chandra, D.; Paolone, A. Temperature dependence of the Elastic Modulus of $(Ni_{0.6}Nb_{0.4})_{1-x}Zr_x$ Membranes: Effects of Thermal Treatments and Hydrogenation. *Energies* **2015**, *8*, 3944–3954. [CrossRef]

28. Palumbo, O.; Paolone, A.; Rispoli, P.; Cantelli, R.; Autrey, T. Decomposition of NH_3BH_3 at sub-ambient pressures: A combined thermogravimetry–differential thermal analysis–mass spectrometry study. *J. Power Sources* **2010**, *195*, 1615–1618. [CrossRef]

29. Palumbo, O.; Trequattrini, F.; Vitucci, F.M.; Bianchin, A.; Paolone, A. Study of the hydrogenation/dehydrogenation process in the Mg-Ni-C-Al system. *J. Alloys Compd.* **2015**, *645*, S239–S241. [CrossRef]

30. Recommended Best Practices for the Characterization of Storage Properties of Hydrogen Storage Materials: V3.34 21 February 2012. Available online: https://energy.gov/eere/fuelcells/downloads/recommended-best-practices-characterization-storage-properties-hydrogen-0 (accessed on 9 February 2017).